Cross-Sectional Analysis of Rib Fracture Mechanism of Elderly Occupant in Frontal Collision using THUMS

Yoshiki Takahira, Satoshi Akima, Yoshito Kusuhara, Noboru Tanase, Yuichi Kitagawa

Abstract An elderly occupant model was generated from THUMS Version 4.1 AM50 occupant model by modifying the material properties and geometries of the ribcage to represent those of a 70-year-old (YO) male person and was validated using Post Mortem Human Subject (PMHS) tests. A vehicle frontal collision simulation was conducted, assuming a collision speed of 56 km/h, using the elderly occupant model. The simulation model predicted fractures in the sternum, clavicle and upper ribs. The location of rib fractures was along the seatbelt path. This was consistent with the fracture pattern observed in the PMHS tests. The amount of contact force from the seatbelt to the chest was greater than that from the airbag to the chest, indicating that the seatbelt force contributed more to the rib fractures. As the occupant upper body flexed due to the inertia, the vertical component of the seatbelt force acting on the upper ribs increased. The cross-sectional analysis of the moment inside the ribs suggested that the upper rib fractures were primarily caused by torsion and superior-inferior bending rather than by anterior-posterior deflection, which was commonly thought to be the indicator.

Keywords Elderly occupant, Human body FE model, Rib fracture, Vehicle frontal collision simulation.

I. INTRODUCTION

In recent years, the proportion of elderly people involved in road traffic injuries and deaths has increased, particularly in Japan and Europe [1-2], and a further increase is expected in the future. The National Highway Traffic Safety Administration (NHTSA) reported that the risk of severe injuries, i.e. 4+ on the Abbreviated Injury Scale (AIS), increases with age [3]. It also reported that the risk of AIS3+ chest injury in frontal collisions is more affected by age compared with other body regions [4]. Among chest injuries, pulmonary contusion and pneumothorax are common and are often associated with rib fractures [5]. It reported that the strength and cross-sectional area of the cortical bone reduce along with the age-related decrease of the bone mineral density [6-8]. In past studies, chest impact tests and table-top belt-loading tests using PMHS were conducted to investigate the chest injury responses. The test results commonly showed that the number of rib fractures increased with the age of the PMHSs [9-11]. On the other hand, the anthropomorphic test dummies (ATDs) used in the crash safety regulations and in the New Car Assessment Programs (NCAP) do not simulate the rib fractures of the human body, and instead use the maximum chest deflection to estimate the occupant risk of rib fractures. For the THOR dummy, the maximum chest deflection (Rmax) is calculated from the resultant deflections measured at four different points on the dummy ribs. Recently, new injury predictors have been proposed that take into account asymmetric deformation of the ribcage, ex. PC-Score and TIC [12-13]. However, few studies have investigated the forces acting on the ribs in frontal collision or analysed the location and timing of rib fractures or the relationship with external forces. A finite element (FE) approach is effective for understanding the impact kinematics and crash-induced injuries of the human body. Some studies reported the reproduction of rib fractures in laboratory tests using the human body FE model [14-15], but few studies reported the reproduction of rib fractures under vehicle seatbelt conditions. In this study, rib fractures of PMHSs in vehicle frontal collision sled test conducted by Albert *et al*. were reproduced using THUMS [16-17]. We also analysed the external force applied to the occupant's chest and the internal force acting on the ribs, and explained the possible mechanism of rib fracture of elderly occupants under vehicle seatbelt conditions.

Y. Takahira is Assistant Manager (e-mail: yoshiki_takahira@mail.toyota.co.jp; tel: +81 50 3192 0175), S. Akima and Y. Kusuhara are Engineers, N. Tanase is Project Manager, Y. Kitagawa, Ph.D., is Chief Professional Engineer in Mobility Evaluation and Engineering Division at Toyota Motor Corporation in Toyota, Japan.

II. METHODS

The simulations were performed using FE models. The LS-DYNA™ Version 971 was used for the FE analysis solver developed by Livermore Software Technology Corporation (US). The FE models consisted of occupant models and vehicle models, including seats and restraint systems.

Occupant Model

The THUMS Version 4.1 AM50 occupant model, as shown in Fig. 1, was used in the vehicle frontal collision simulations. It corresponds to a midsize male occupant with a height of 178.6 cm and a weight of 77.6 kg. The model describes the anatomical features of human body, including the major skeletal parts, articular ligaments, brain, internal organs and other soft tissue parts. THUMS' mechanical responses were validated for various loading cases using PMHS test data described in the literature [18-21]. In this study, the ribcage of THUMS was modified as shown in Fig. 2. The insertion point of the costoclavicular ligament was extended from the original one so as to cover the anterior-superior part of the 1st rib with reference to the anatomy. The boundary lines between the costal cartilage and the costal bones were moved to the anterior direction, to better represent the average length of the costal cartilage as shown in the literature [22].

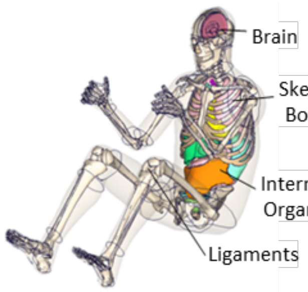

Fig. 1. THUMS Version 4.1 AM50 occupant model.

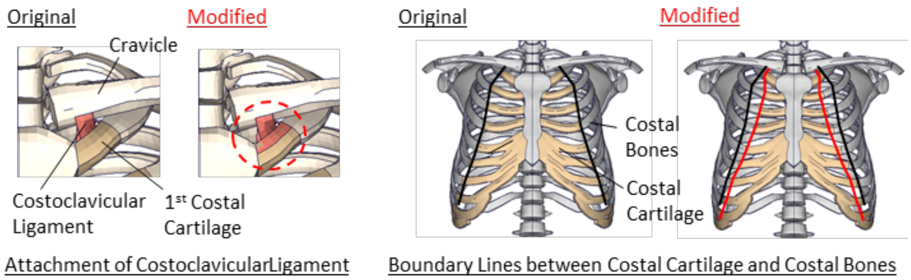

Fig. 2. Modifications of the ribcage model.

Age-related Model Preparation

THUMS AM50 was developed as a representative of age 30s. In this study, THUMS AM50 was assumed to be 35YO. The ribcage characteristics of 70YO human were applied to the ribcage part in THUMS. The material property, thickness of the cortical bone and the ribcage angle in lateral view were selected as age-related parameters, as shown in Fig. 3. The cortical bone stress-strain curves scaled yield and fracture points from 35YO to 70YO and reduced fracture strain by 37%, based on the data measured by Courtney *et al.* and McCalden *et al.* [6-7]. The cortical bone thickness of ribs and clavicles was reduced by 28% to represent those of 70YO, based on the measurement of rib cross-sectional area performed by Stein *et al.* [8]. The cortical bone thickness of the sternum was reduced from 1 mm (35YO) to 0.4 mm (70YO) to fit the corridor of the age and fracture force created by Ito *et al*. [23]. It was based on the measurement of fracture force of the sternum in the three-point bending tests conducted by Kerrigan *et al*. [24]. The ribcage angle with respect to the spine in lateral view was increased by 4 degrees upward from 35YO to 70YO, based on the study of Kent *et al*. [25].

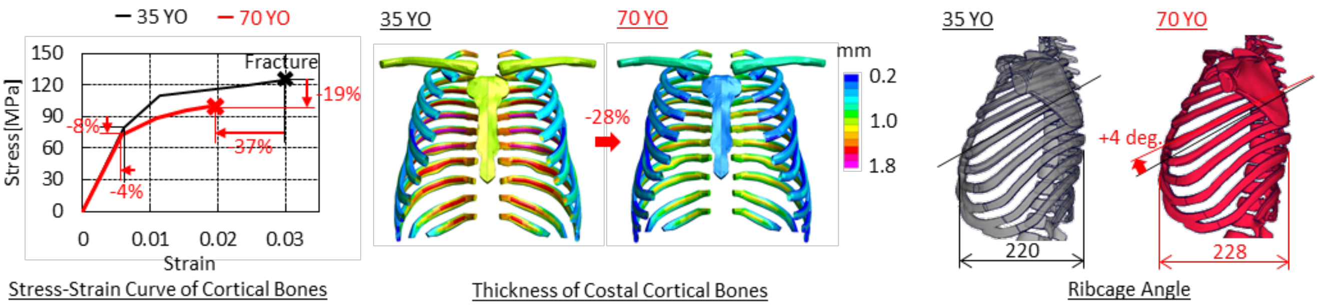

Fig. 3. Age-related parameters of the ribcage characteristics.

Vehicle Frontal Collision Simulation Model

Figure 4 shows the simulation model used in this study. It represented a prototype midsize sedan with THUMS positioned in the driver's seat. The vehicle interior was almost same as the one used for the PMHS tests conducted by Albert *et al*. [16-17]. An acceleration pulse of a frontal collision at a speed of 56 km/h was applied to the model. The interior parts (steering, instrument panel, pedals, seats, seatbelt and airbags) that could come into contact with the occupants were assumed to be deformable, while the windshield and floor panel were assumed to be rigid. The seatbelt retractor model simulated the functions of a pre-tensioner and a load-limiter. The deployment of the driver airbag (DAB) and knee airbag (KAB) was also simulated. (The foam with almost the same stiffness as the KAB was used in the PMHS tests.)

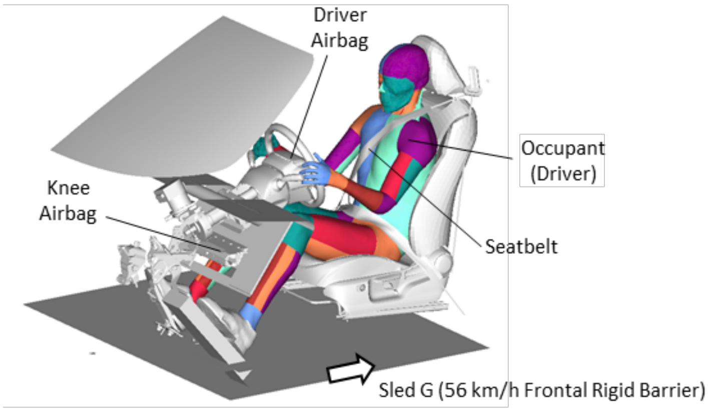

Fig. 4. Vehicle frontal collision model.

Simulation Matrix

A total of four simulations were conducted with the age-related parameters: (i) Stress-strain curve of cortical bones, (ii) Thickness of cortical bones and (iii) Ribcage angle in lateral view, as shown in Table I. Case 1 assumes an elderly occupant. The purpose was to validate THUMS elderly occupant model to the literature data. The impact kinematics and rib fracture location were examined. Comparison was made between the simulation results of Case 1 and the PMHS test results in which the average age was 70YO. The purpose of running Case 3 and Case 4 was to understand the contribution of each parameter to the rib fractures. In the second part of the study, the mechanism of rib fracture was investigated. The external force applied to the chest and the internal force acting on the ribs of elderly and non-elderly were compared and analysed. Case 2 assumes a non-elderly occupant (35YO).

TABLE I
SIMULATION MATRIX

Parameter	Case 1	Case 2	Case 3	Case 4
(i) Stress-Strain curve of Cortical Bones	70 YO	35 YO	70 YO	70 YO
(ii) Thickness of Cortical Bones	70 YO	35 YO	35 YO	70 YO
(iii) Rib Angle	70 YO	35 YO	35 YO	35 YO

Post-processing of Simulation Result

The 3D coordinate data of all nodes and the strain values calculated for all elements were extracted every 2 milliseconds (ms). Time history data, such as displacement calculated on the selected node, was output every 0.1 ms. Post-processing software Animater^{TM} and LS-PrePost^{TM} were used to visualize the impact kinematics of the occupant model and plot the time history curve. The impact kinematics was analysed in the vehicle coordinate system. The nodal time history data of anatomical landmarks on THUMS were output and compared to those measured in the PMHS tests. The landmark points were the head centre of gravity (COG), left shoulder point and left hip point. The PMHS sled tests were conducted under three conditions: Spec. 1 with DAB and KAB;

Spec. 2 with DAB without KAB; and Spec. 3 without DAB or KAB [16-17]. Note that Spec. 1 assumes the same condition as the simulation. The results of the three PMHS tests with Spec. 1 were used to compare the impact kinematics of the THUMS elderly model. The number of the fractured bones which included at least one eliminated element in the simulation were compared with the fracture frequency in the PMHS tests. The fracture frequency of PMHS tests was calculated by dividing the number of the full fractures in each bone by the total number of PMHS in all test conditions (Spec. 1-3). The average age of PMHS was 70YO (excluding the 88YO PMHS, who had an extremely high number of fractures). The contact forces between the occupant's body and the restraint system, such as driver airbags, seatbelts and seats, were calculated. The chest deflection ratio was calculated to investigate the relationship with the rib strain. The chest deflection ratio was defined as a changed ratio of the distance between the anterior point and the posterior point at the left superior and right inferior chest on the seatbelt path, as shown in Fig. 5. The moments of torsion component: M_X, superior-inferior bending component: M_Y and anterior-posterior deflection component: M_Z defined in the local coordinate system of each rib cross-section – were investigated, as shown in Fig. 6, to understand the mechanism of rib fracture. An index A, representing the moment of the cross-sectional strength ratio, was calculated, as shown in Fig. 7. The index A based on von Mises yield criterion was defined by dividing each moment component by the respective total cross-sectional plastic moment, and dividing the sum of squares by the square root by the constant α. The constant α was the ratio of fracture stress σ_F to yield stress σ_P of the cortical bone.

Fig. 5. Chest deflection ratio measuring points.

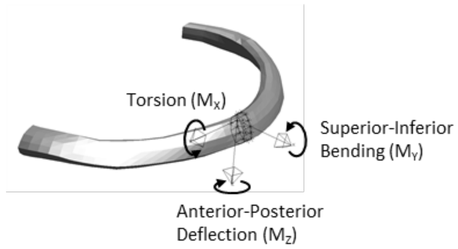

Fig. 6. Definition of cross-sectional moment. Example of left 2nd rib.

Index A

$$A = \sqrt{\left(\frac{M_X}{M_{PX}}\right)^2 + \left(\frac{M_Y}{M_{PY}}\right)^2 + \left(\frac{M_Z}{M_{PZ}}\right)^2} \Big/ \alpha$$

$$\alpha = \sigma_F / \sigma_P$$

M_{PX}: Full Plastic Moment for M_X
M_{PY}: Full Plastic Moment for M_Y
M_{PZ}: Full Plastic Moment for M_Z
σ_F: Fracture Stress
σ_P: Yield Stress

Rib Properties (Example of Left 2nd Rib)

	M_{PX}	M_{PY}	M_{PZ}	σ_F	σ_P
Case 1	4.8 Nm	6.7 Nm	5.0 Nm	99.7 MPa	73.3 MPa
Case 2	6.9 Nm	9.7 Nm	7.2 Nm	124.5 MPa	79.9 MPa

Fig. 7. Definition of Index A, representing the moment of the cross-sectional strength ratio.

III. RESULTS

Validation of Elderly Model

Figure 8 shows the occupant kinematics in a lateral view in the simulation of Case 1 assuming an elderly occupant. The time frames at 0 ms, 75 ms and 95 ms were selected. The pelvis (hip point) forward displacement reached the maximum value with respect to the vehicle at 75 ms, while the displacements of the head and shoulder point reached the maximum at 95 ms. The maximum forward displacement was 485 mm for the head, 332 mm for the shoulder point, and 127 mm for the hip point. Figure 9 compares the time history curves of forward displacement of the occupant's head, shoulder point, and hip point between the PMHS test results and the simulation results of Case 1. The simulation results were almost within the range of the PMHS test results.

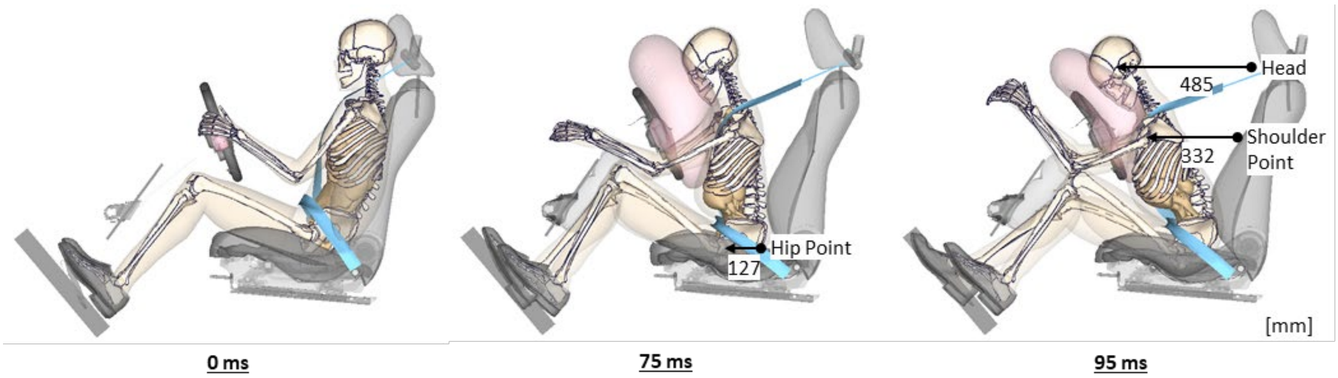

Fig. 8. Occupant kinematics of THUMS in simulation (Case 1).

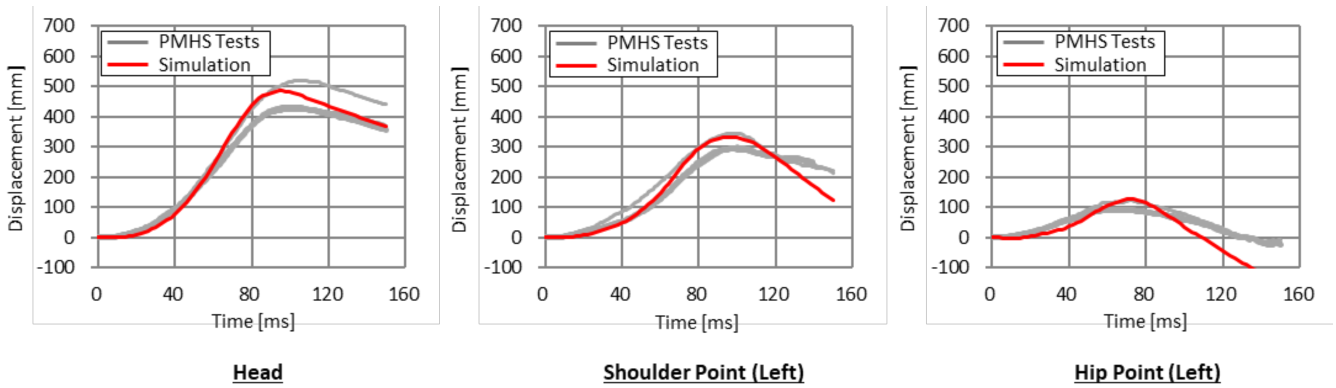

Fig. 9. Comparison of occupant displacement between PMHS and THUMS (Case 1).

Figure 10 shows the frequency and location of fractured ribs in the PMHSs, the distribution of the maximum rib strain and the location of fractures (element elimination) in the simulations. THUMS ribcage strain distributions were obtained by dividing the maximum equivalent strain ε of each element by the failure strain ε_F. In Case 1 (elderly occupant), the simulation indicated fractures of the sternum, clavicle, left 2nd rib, and left 3rd rib. These locations corresponded to the frequent fracture bones in the PMHS tests. No right rib fractures were observed, however high strain occurred at the right 6th rib. In Case 3, where only the material properties of the ribcage were changed from Case 2 (non-elderly), fracture occurred only in the left 2nd rib. In Case 4, where the thickness of ribcage was changed from Case 3, the fracture location was the same as Case 1.

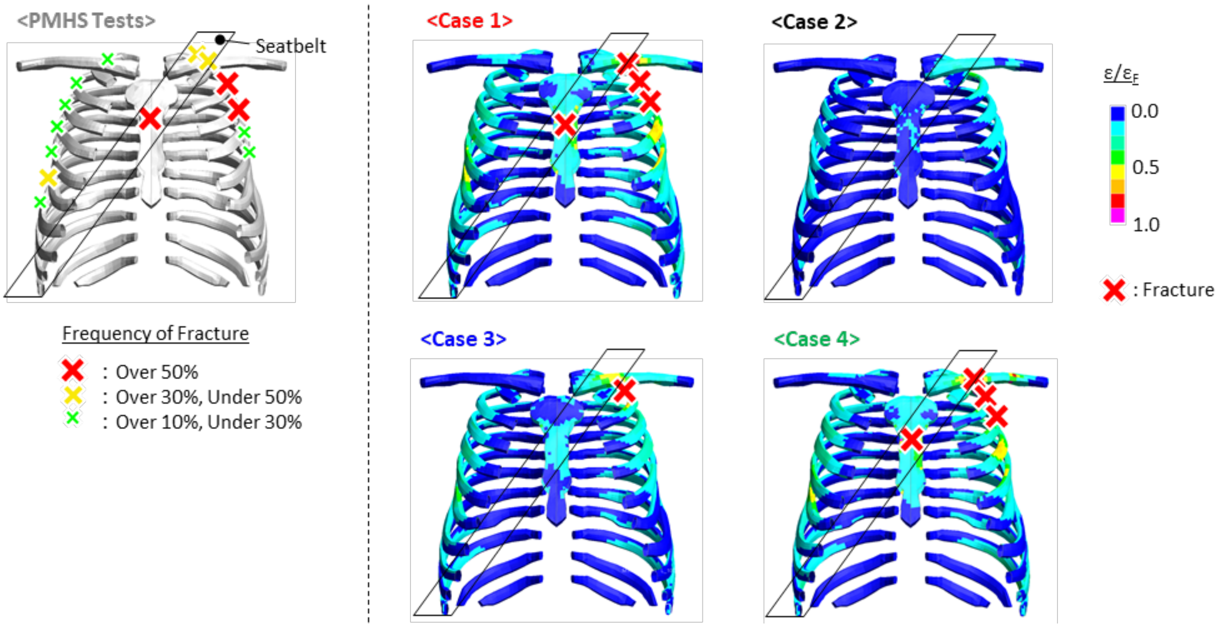

Fig. 10. Frequency of fractures in PMHS tests and distribution of maximum rib strain in simulations.

Mechanism of Rib Fracture

The simulation results of Case 1 (elderly occupant) and Case 2 (non-elderly occupant) were compared in order to understand the mechanism of rib fracture. Figure 11 shows the force-displacement curves. The force in the vertical axis indicates the external force applied to the chest, while the displacement in the horizontal axis indicates the chest (T4) forward displacement. The left plot shows the result of Case 1 and the right plot shows the result of Case 2. In both simulations, the maximum seatbelt force was about 5.5 kN, the maximum DAB force was about 3.8 kN, and the maximum forward displacement of the chest was about 350 mm. The contact force from seatbelt force was greater than that from the DAB. In the simulation of Case 1, the sternum and clavicle were fractured at around a chest displacement of 100 mm, and the left 2nd rib and left 3rd rib were fractured at around a chest displacement of 300 mm. Figure 12 plots the growth of rib strain with respect to chest deflection ratio. The left plot shows the result of Case 1 and the right plot shows the result of Case 2. The solid line shows the curve of the left 2nd rib strain in which the fracture occurred in Case 1 versus the left superior chest deflection ratio. The dashed line shows the curve of the right 6th rib strain without fractures in both cases versus the right inferior chest deflection ratio. The red X indicates the time fracture occurred. In both cases, the strain of the right 6th rib increased with the chest deflection rate. By contrast, the strain of the left 2nd rib increased more slowly than the right 6th rib, but increased suddenly at a deflection ratio of around 0.15.

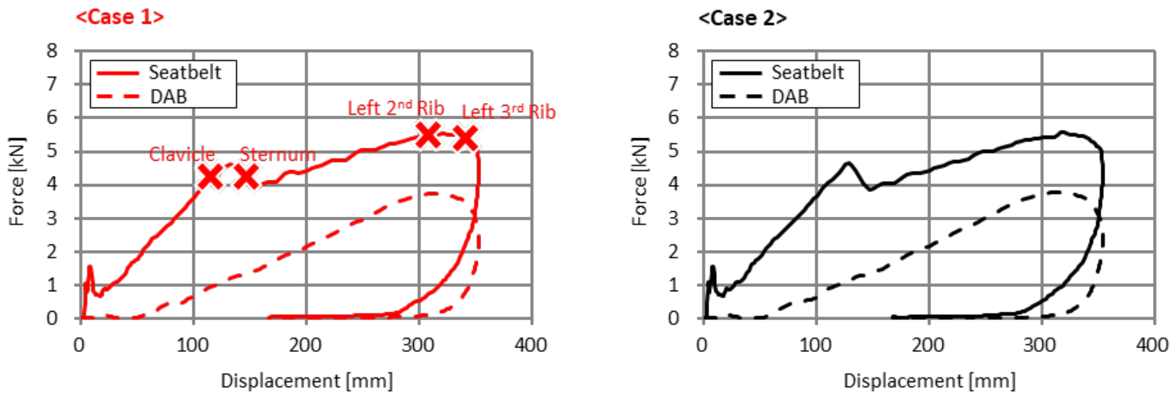

Fig. 11. Contact force from seatbelt and DAB-chest displacement curve.

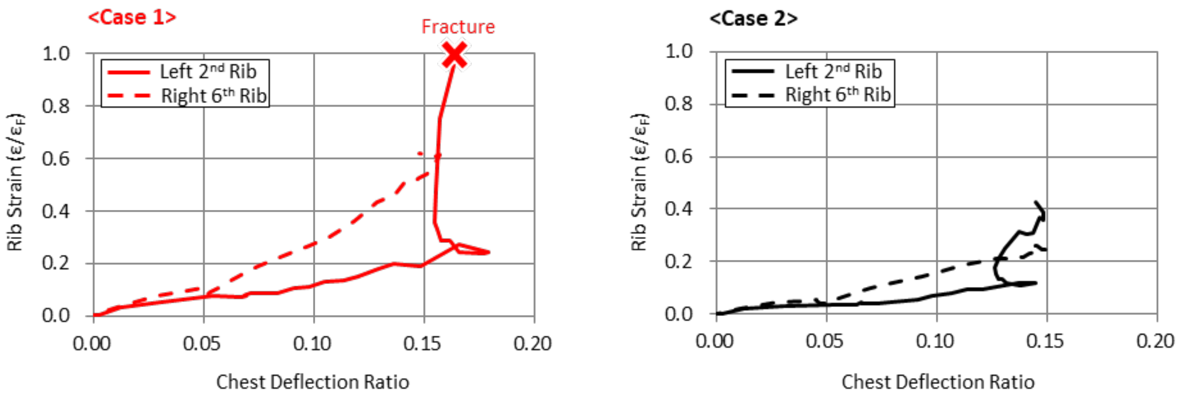

Fig. 12. Rib strain – chest deflection ratio curve.

The study analysed the moment acting on the rib cross-section to understand the reason for the weak correlation between the left 2nd rib strain and the chest deflection rate. Figure 13 shows the time history curves of the moment in the cross-section where the maximum strain occurred in the left 2nd rib. The left plot shows the result of Case 1 and the right plot shows the result of Case 2. In both cases, M_X and M_Y increased at around 60 ms while M_Z decreased. In Case 1, the rib fractured at a moment lower than the maximum value in Case 2. Figure 14 shows an index A, representing the moment of the cross-sectional strength ratio at the timing when the moment of the left 2nd rib became maximum. In both cases, the proportions of the torsional component M_X were largest, at 49% and 51%, respectively. The index A in Case 1 reached 1.0, and the rib fractured.

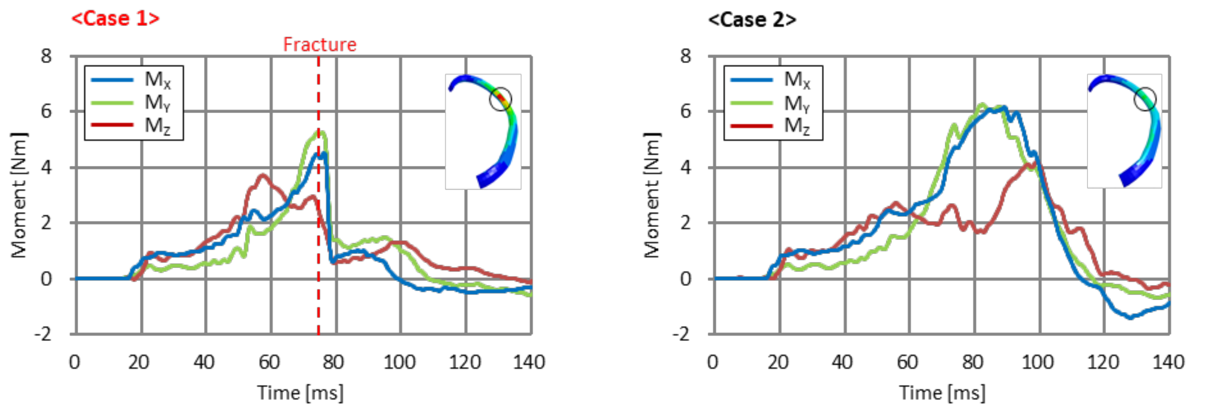

Fig. 13. Moment around left 2nd rib.

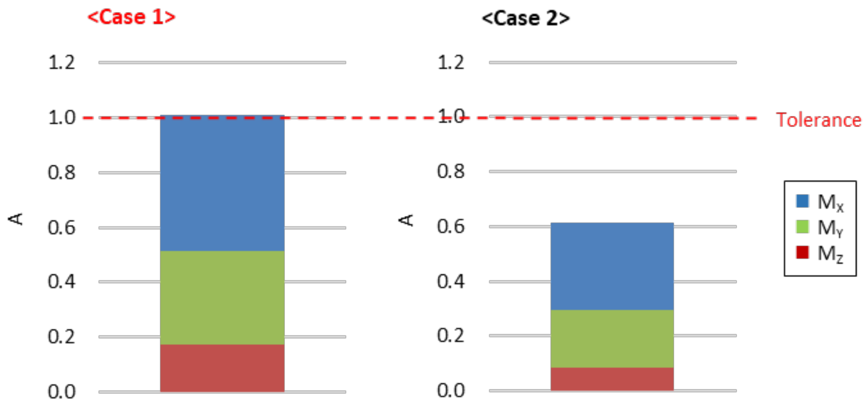

Fig. 14. Index A in left 2nd rib.

The study also investigated the external forces applied to the left 2nd rib in order to understand the cause of the torsional moment acting on the left 2nd rib. Figure 15 shows the vectors of contact force between the seatbelt and the upper left chest at the timing when the left 2nd rib fractured in the simulation of Case 1. The magnitude of the vector represents the force per unit element. Around the left 2nd rib, a downward contact force was applied from the seatbelt to the parallel to the rib on the anterior (F_1) and the posterior (F_2) of the rib. Figure 16 shows the distribution of the contact force applied to the left 2nd rib in the top view of the rib. The coordinate system in the figure represents the local coordinate defined for the fracture cross-section. The centre of the contact force F_1 on the anterior of the rib was away from the X'-coordinate by a distance L_1, where the X'-coordinate of the fracture cross-section was defined on the side of the rib. The torsional moment acting on the fracture cross-section was calculated as $M_X = F_1 * L_1 = 4.6$ Nm, which was almost the same as the moment measured on the cross-section shown in Fig. 13.

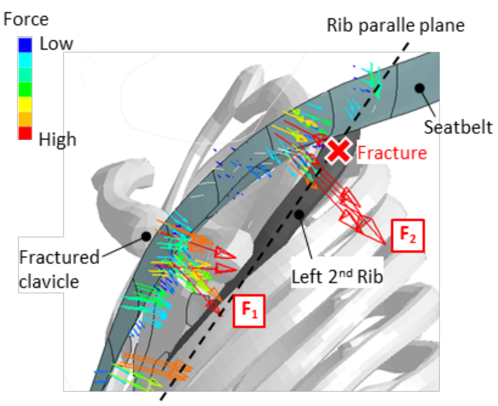

Fig. 15. Contact force vector around left 2nd rib at fracture timing (Case 1).

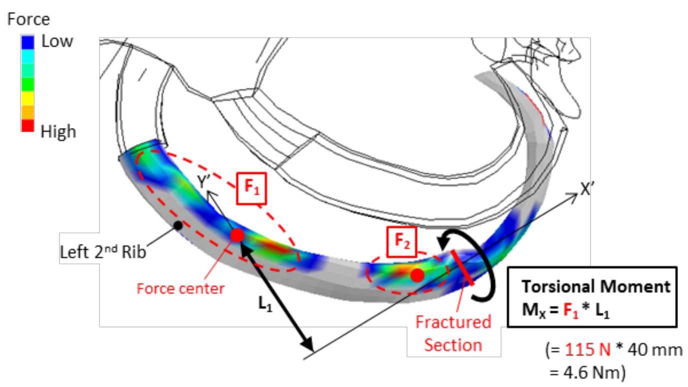

Fig. 16. Contact force distribution of left 2nd rib at fracture timing in top view of rib parallel plane (Case 1).

IV. Discussion

The frontal collision simulation using the elderly occupant model (Case 1) predicted fracture of the clavicle, sternum, left 2nd rib, and left 3rd rib where high frequency of fracture was reported in the PMHS sled tests. Of the three parameters selected as ribcage characteristics changing with age, the stress-strain curve and thickness of cortical bone contributed to rib fracture, with a limited contribution of the ribcage angle in lateral view. According to the study by Kent *et al.*, the ribcage angle was more correlated with BMI than with age [24]. Further research is necessary to better understand the relationship between ageing and BMI.

Regarding the force applied to the chest from the seatbelts-DAB and the forward displacement of the chest, there was little difference between the elderly model (Case 1) and the non-elderly model (Case 2). The seatbelts had a larger force applied to the chest compared with the DAB and contributed more to rib fractures. The contact force from the seatbelt increased with the forward displacement of the chest. The sternum and clavicle fractured at an early timing of collision while the upper ribs fractured at a late timing of collision in the simulation of Case 1. The contact force from the seatbelt increased while the seatbelt tension around the shoulder was kept constant by the load limiter. This is because the seatbelt wrapping angle decreases as the upper body moves forward, and the seatbelt contact force is geometrically proportional to the cosine of the wrapping angle, as shown in Fig. 17. A strong correlation was found between the strain of lower ribs (the right 6th rib) and the chest deflection rate, while the correlation was weak for the upper ribs (the left 2nd rib). The main cause of this was that the vertical component of the contact force applied to the upper ribs increased as the occupant upper body flexed due to the inertia, and the force acted as a torsional moment on the cross-section of the side of the rib. While the magnitude of the moment acted on the rib of the elderly model (Case 1) was smaller than that of the non-elderly model (Case 2), the rib fracture occurred by the reduction of cross-sectional strength due to the decrease of the cortical bone thickness.

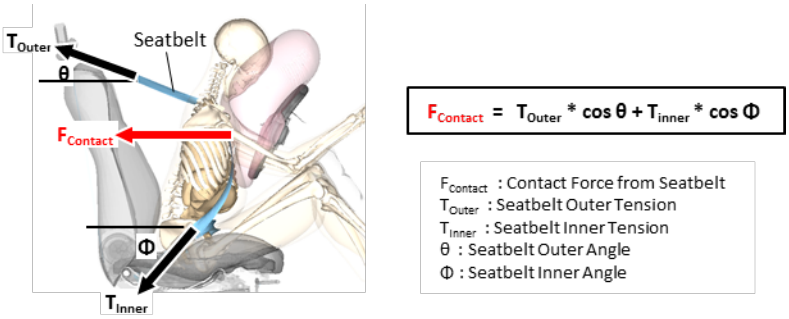

Fig. 17. Relationship between seatbelt contact force and tension.

V. Limitations

This study assumed equivalent characteristics of non-ribcage cortical bones, costal cartilages and soft tissues for the elderly model and the non-elderly model. The study also assumed a particular sitting posture and position for each occupant model, but of course this may vary among individuals and in specific situations. Interaction with restraint systems is also influenced by such factors.

VI. Conclusions

An FE model of an elderly male occupant was generated by changing the ribcage characteristics of the non-elderly (THUMS Version 4.1 AM50) occupant model to those of 70YO. A frontal collision simulation was performed using the elderly model to replicate a physical sled test with PMHS. The location of the rib fractures predicted in the simulation correlated well with the PMHS test results. The analysis results suggested that the upper rib fractures were primarily caused by the torsion and superior-inferior bending of the rib rather than by anterior-posterior rib deflection generally measured. The torsion and superior-inferior bending of the rib was caused by the increase of the vertical component of seatbelt contact force created with the upper body flexion.

VII. REFERENCES

[1] National Police Agency (Japan). *Annual Report on Number of fatalities in traffic accidents in 2020* (in Japanese), Internet: https://www.npa.go.jp/publications/statistics/koutsuu/toukeihyo.html, accessed 4 January 2021.

[2] United Nations Economic Commission for Europe (ENECE). Persons Killed or Injured in Road Traffic Accidents (1994-2018), Internet: https://w3.unece.org/PXWeb/en.

[3] Liu, C., Utter, D., Chen, C. (2007) Characteristics of Crash Injuries Among Young, Middle-Aged, and Older Drivers. *NHTSA Technical Report*, DOT HS 810 857.

[4] Ridella, S., Rupp, D., Poland, K. (2012) Age-Related Differences in AIS 3+ Crash Injury Risk, Types, Causation and Mechanisms. *Proceedings of IRCOBI Conference*, 2012, Dublin, Ireland.

[5] Tominaga, S., Nishimoto, T., Motomura, T., Mashiko, K., Sakamoto, Y. (2012) Analysis of Thoracoabdominal Injury based on Japan Trauma Data Bank and In-depth Accident Study. *Transactions of Society of Automotive Engineers of Japan*, **43**(2): pp.269–274.

[6] Courtney, C., Hayes, C., Gibson, J. (1996) Age-Related Differences in Post-Yield Damage in Human Cortical Bone. Experiment and Model. *Journal of Biomechanics*, **29**(11): pp.1463–1471.

[7] McCalden, R. W., McGeough, J. A., Barker, M. B., Court-Brown, C. M. (1993) Age-Related Changes in The Tensile Properties of Cortical Bone. *Journal of Bone and Joint Surgery*, **75-A**: pp.1193–1205.

[8] Stein, I., Granik, G. (1976) Rib Structure and bending strength: an autopsy study. *Calcified tissue research*, **20**: pp.61–73.

[9] Kroell, C., Schneider, D., Nahum, A. (1971) Impact tolerance and response of the human thorax. Technical Paper 710851, *Proceedings of the SAE International Congress and Exposition*, 1971, Detroit, USA.

[10] Kroell, C., Schneider, D., Nahum, A. (1974) Impact tolerance and response of the human thorax II. Technical Paper 741187, *Proceedings of the SAE International Congress and Exposition*, 1974, Detroit, USA.

[11] Cesari, D., Bouquet, R. (1990) Behavior of Human Surrogates Thorax under Belt Loading. Technical Paper 902310, *Proceedings of the SAE International Congress and Exposition*, 1990, Detroit, USA.

[12] Poplin, G., McMurry, T., *et al*. (2017) Development of thoracic injury risk functions for the THOR ATD. *Accident Analysis and Prevention*, **106**: pp.122–130.

[13] Xavier, T., Pascal, B. (2019) Updated Chest Injury Criterion for the THOR. *Proceedings of the 26st ESV Conference*, 2019, Eindhoven, Netherlands.

[14] Kawabuchi, T., Takahashi, Y. (2018) Verification of Rib Fracture Prediction in Frontal Collision with Human Body Models Representing Specific Ages. *Proceedings of IRCOBI Conference*, 2018, Athens, Greece.

[15] Jin, X., Kalra. A, *et al*. (2018) Development and Validation of Whole-Body Finite Element Occupant and Pedestrian Models of a 70-Year-Old Female. *Proceedings of IRCOBI Conference*, 2018, Athens, Greece.

[16] Albert, D., Beeman, S., Kemper, A. (2018) Occupant kinematics of the Hybrid III, THOR-M, and postmortem human surrogates under various restraint conditions in full-scale frontal sled tests. *Traffic Injury Prevention,* **19**(S1): pp.S50–S58.

[17] Albert, D., Beeman, S., Kemper, A. (2018) Assessment of Thoracic Response and Injury Risk Using the Hybrid III, THOR-M, and Post-Mortem Human Surrogates under Various Restraint Conditions in Full-Scale Frontal Sled Tests. *Stapp Car Crash Journal*, **62**: pp.1–65.

[18] Watanabe, R., Miyazaki, H., Kitagawa, Y., Yasuki, T. (2012) Research of the relationship of pedestrian Injury to collision speed, car-type, impact location and pedestrian sizes using human FE model (THUMS Version 4). *Stapp Car Crash Journal*, **561**: pp.269–32.

[19] Shigeta, K., Kitagawa, Y., Yasuki, T. (2009) Development of next generation human FE model capable of organ injury prediction. *Proceedings of the 21st ESV Conference*, 2009, Stuttgart, Germany.

[20] Kitagawa, Y., Yasuki, T. (2013) Correlation among seatbelt load, chest deflection, rib fracture and internal organ strain in frontal collisions with human body finite element models. *Proceedings of IRCOBI Conference*, 2013, Gothenburg, Sweden.

[21] Kitagawa, Y., Hayashi, S., Yamada, K., Gotoh, M. (2017) Occupant kinematics in simulated autonomous driving vehicle collisions, direction and angle. *Stapp Car Crash Journal*, **61**: pp.101–155.

[22] Holcombe, S., Brown, E., Wang, S. (2020) Building a better rib. *Proceedings of the JSAE Annual Congress (Spring),* 2020.

[23] Kerrigan, J., Bose, D., *et al*. (2010) Response of the sternum under dynamic 3-point bending. *ISA Volume 480 Biomedical Sciences Instrumentation*, **46**: pp.342–347.

[24] Ito, O., Ito, Y., Dokko, Y., Mori, F., Ohhashi, K. (2011) Development of Adult and Elderly Thorax Models (Second Report). *Transactions of Society of Automotive Engineers of Japan*, **42**(3): pp.703–708.

[25] Kent, R., Lee, S. H., *et al*. (2005) Structural and material changes in the aging thorax and their role in crash protection for older occupants. *Stapp Car Crash Journal*, **49**: pp.231–249.